

Title	Role of base in the formation of silver nanoparticles synthesized using sodium acrylate as a dual reducing and encapsulating agent
Author(s)	Nishimura, Shun; Mott, Derrick; Takagaki, Atsushi; Maenosono, Shinya; Ebitani, Kohki
Citation	Physical Chemistry Chemical Physics, 13(20): 9335-9343
Issue Date	2011-04-08
Type	Journal Article
Text version	author
URL	<a href="http://hdl.handle.net/10119/10734">http://hdl.handle.net/10119/10734</a>
Rights	Copyright (C) 2011 Royal Society of Chemistry. Shun Nishimura, Derrick Mott, Atsushi Takagaki, Shinya Maenosono and Kohki Ebitani, Physical Chemistry Chemical Physics, 13(20), 2011, 9335-9343. <a href="http://dx.doi.org/10.1039/C0CP02985H">http://dx.doi.org/10.1039/C0CP02985H</a> - Reproduced by permission of The Royal Society of Chemistry
Description	

# Role of Base in the Formation of Silver Nanoparticles Synthesized Using Sodium Acrylate as Dual Reducing and Encapsulating Agents

Shun Nishimura,<sup>a</sup> Derrick Mott,<sup>a</sup> Atsushi Takagaki,<sup>b</sup> Shinya Maenosono,<sup>\*a</sup> and Kohki Ebitani<sup>\*,a</sup>

Received (in XXX, XXX) Xth XXXXXXXXX 200X, Accepted Xth XXXXXXXXX 200X

5 First published on the web Xth XXXXXXXXX 200X

DOI: 10.1039/b000000x

The formation mechanism of Ag nanoparticles (NPs) synthesized with a wet-chemical reduction method using sodium acrylate as dual reducing and capping agents was investigated with various analytical techniques. The time course of state of the reaction solution was investigated using UV-  
10 vis and XAFS spectroscopies which showed that the NP formation rate increased with increasing concentration of sodium hydroxide (NaOH). The detailed kinetic analyses reveal that both the reduction rate of Ag ions and the nucleation rate of Ag NPs are dramatically increased with increasing the NaOH concentration. XANES analyses imply that another reaction pathway *via* alternative Ag<sup>+</sup> species, such as Ag(OH)<sub>x</sub>, was developed in the presence of NaOH. Consequently,  
15 NaOH is found to play an important role not only in creating specific intermediates in the reduction of Ag<sup>+</sup> to Ag<sup>0</sup>, but also accelerating the reduction and nucleation rates by enhancing the oxidation of sodium acrylate, thereby increasing the rate of formation of the Ag NPs.

## Introduction

A wet chemical reduction method has been widely employed  
20 for the preparation of highly dispersed nanoparticles (NPs), because it is relatively simple and has wide applicability in synthesis of various types of NPs. The synthetic procedure involves the reduction reaction of one or more metal precursors in the presence of capping ligands using a reducing  
25 agent such as hydrogen, formaldehyde, sodium borohydride, hydrazine or  $\gamma$ -irradiation. Some organic materials such as poly(allylamine) (PAAm), poly(*N*-vinyl-2-pyrrolidone) (PVP), poly(vinyl alcohol) (PVA), poly(sodium acrylate) (PSA), poly(ethylene glycol) (PEG), citric acid, ascorbic acid, and  
30 glucose have been employed as dual active agents,<sup>1</sup> serving as both reducing and capping agent in the method.

Many researchers have focused on the control of NP size and shape, because these have a strong relationship with the properties, for example as catalyst, magnetic devices,  
35 biosensors, and so on. There are several successful reports on the synthesis of NPs which show the effect of solvent polarity,<sup>2</sup> shape directing agents,<sup>3</sup> or mixing ratio of metal precursor to stabilizer,<sup>4</sup> on the metal NP formation. Although the relationships between the synthesized metal NPs  
40 morphology and preparation conditions have been gradually clarified, it is still difficult to design a novel synthetic methodology in a rational manner to obtain highly uniform and size/shape controllable metal NPs. This is mostly because the NP formation process is generally governed by an  
45 instantaneous nucleation process followed by crystal growth. The nucleation and growth rates nonlinearly depend on the supersaturation of atoms, and have a profound effect on the mean size, size distribution and morphology of the resulting NPs. This means that the control of supersaturation of atoms  
50 is crucially important to obtain highly monodisperse and shaped NPs. The supersaturation of atoms is closely related to

the reduction rate of ions, complexation ability of capping ligands with metal, and solubility and stability of intermediates. It remains a mystery how intermediates are  
55 formed during the reaction and how they affect the reaction kinetics.

The X-ray adsorption fine structure (XAFS) method is a valuable technique for providing information of the dynamic aspect of the particle formation. Regarding the formation  
60 mechanism of highly monodisperse NPs, Polte and coworkers investigated the Au NP formation process by XAFS and small-angle X-ray scattering (SAXS) methods using synchrotron radiation, and they found that the Au NPs were formed over a four step mechanism as follows: fast initial  
65 nucleation, coalescence of the nuclei into bigger particles, slow further growth, and fast final growth.<sup>5</sup> Harada *et al.* studied the formation mechanisms of Rh, Pd, Ag, Au, and Pt NPs synthesized by photoreducing metal ions in an aqueous ethanol solution and they found that the type of formed seed  
70 and/or intermediates during reduction were strongly related to the formation kinetics of NPs.<sup>6</sup> Very recently, we investigated the formation mechanism of Cu NPs using the *in situ* XAFS method with other supporting techniques, and proposed that the role of PVP in the Cu NP formation is primarily as a  
75 stabilizer, not only for the formed NPs but also for intermediates such as Cu<sup>+</sup> ions and Cu hydroxides, which prolongs the lifetime of Cu<sup>+</sup> ion and reduces the supersaturation of Cu<sup>0</sup> species, during the course of the reaction.<sup>7</sup>

80 Ag NPs are one of the most attractive materials for electric devices, catalysts, antibacterial agents, fluorescent labels and bio/chemical sensing applications. Recently, we developed a synthetic methodology towards fine Ag NPs with narrow size distribution using sodium acrylate as dual reducing and  
85 encapsulating agent (See Electronic Supplementary Information (ESI)†, Fig. S1).<sup>8</sup> In our own synthesis approach to Ag NPs, the addition of NaOH is known to have a large

impact on the reaction kinetics of particle formation, and is thought to be the key factor in regulating the monodispersity of the resulting Ag NPs. However, until now, the formation mechanism has not been well understood. Although some people have studied the formation process of Ag NPs synthesized in different ways using UV-vis spectroscopy,<sup>9</sup> there have been no detailed reports on the effect of alkaline agent on the reaction kinetics. Therefore, in this paper, we present a study on the role of NaOH in the formation of Ag NPs using the *in situ* XAFS method in combination with other observation techniques.

## Experimental Section

The Ag NPs were synthesized with a wet-chemical reduction method reported by Mott *et al.*<sup>8</sup> with some modifications. Silver nitrate (AgNO<sub>3</sub>) and sodium acrylate (SA) were used as a precursor and dual reducing/capping agent, respectively. First, a 0.83 mM solution of AgNO<sub>3</sub> was prepared, then sodium hydroxide (NaOH) was gradually dropped into the solution with stirring at room temperature. Second, 5 mL of 50 mM SA was added to the above solution. The prepared solution consisted of AgNO<sub>3</sub>/NaOH/SA with molar ratios of 1/*x*/6.7 in 50 mL water, where *x* was varied in the range of 0–3.6. The solution was refluxed in a two-neck round-bottom glass flask at 373 K under an Ar atmosphere. The solution was sampled several times during the reaction using a clean glass pipette at various times after the start of refluxing at 373 K. The sampled liquid was rapidly-quenched and immediately used for *ex situ* characterizations.

X-ray diffraction (XRD) patterns of solid materials were obtained in reflection geometry using an X-ray diffractometer (Rigaku, RINT2000) at room temperature with Cu K $\alpha$  radiation (wavelength, 1.542 Å; step width, 0.02°). The sample was prepared by centrifuging the solution followed by drying *in vacuo*.

The mean size, size distribution and morphology of NPs were examined using a Hitachi H-7100 transmission electron microscope (TEM) operated at 100 kV. TEM samples were prepared by dropping the reaction solutions onto carbon-coated copper microgrids followed by drying *in vacuo*.

UV-vis spectra were recorded with a Perkin-Elmer Lambda35 spectrometer at room temperature. After the sampling, the solution was diluted to eight times with highly purified water for measurement.

XAFS was obtained at BL01B1 in SPring-8 (proposal No. 2010A1598). The Ag-K edge (K $\alpha$ ; 22.16 keV) XAFS spectra were measured with a fluorescence method using a multi-element solid state detector (SSD). The synchrotron radiation beam was monochromated using Si(311) single crystal. The obtained spectra were treated with count loss correction before analyzing. The  $k^3$ -weighted extended XAFS (EXAFS) functions [ $k^3\chi(k)$ ] were obtained from normalized EXAFS spectra, and Fourier-transformations (FT) were performed within the range  $\Delta k = 3\text{--}11 \text{ \AA}^{-1}$ .

## Results and Discussion

### Visual inspection of the reaction solutions

The colorless AgNO<sub>3</sub> aqueous solution gradually became a yellow cloudy solution during addition of NaOH at room temperature. After that, the injection of SA aqueous solution caused no change in the color. Next, during temperature ramping from room temperature to reflux, the prepared yellowish solution transformed to a paler yellow shade. The color changes of the solutions over time during the reaction after the start of refluxing at 373 K shows the differences in the case of using  $x = 0, 1.1, \text{ or } 3.6$  (Fig. 1). The color of the solutions gradually became deep yellow color *via* a dark blue color (through transmitted light) despite the amount of NaOH added. Hying and coworkers also reported that a dark yellow solution was obtained before a lighter yellow solution in the formation process of Ag NPs reduced by borohydride, and they suggested that the dark yellow solution occurred due to the composition and prismatic qualities of reduced silver.<sup>10</sup> Yin *et al.* also reported a similar color transition in their work.<sup>11</sup> According to these reports, our dark blue (transmitted light) solutions also indicated the existence of small reduced Ag NPs in the formation process. Comparing the color of the solution after 30 min refluxing, the solution synthesized with a high amount of NaOH took on a more deep yellow color than others. It seems that the reduction pathways were not drastically changed, although the rate of reduction is highly affected by the amount of NaOH added in the synthesis.

### Time evolution of absorption spectra of reaction solutions

Figure 2 shows the UV-vis spectra of the solutions after sampling in the cases of  $x = 0, 1.1, \text{ and } 3.6$ . The absorbance peak around 405 nm corresponds to the surface plasmon resonance (SPR) band derived from Ag NPs which possess a small spherical structure (ca. 3–10 nm).<sup>12</sup> In the case of Ag NPs, the intensity of the SPR band is directly related to the amount and size of synthesized Ag NPs, and the SPR peak wavelength is related to the electron density which is associated with different types of adsorbates<sup>13,14</sup> or particle size and shape.<sup>15</sup> Moreover, initial oxidation of surface silver atoms also causes a red shift of the SPR peak because of removal of electron density from the particle surface.<sup>11,14</sup> From TEM and XAFS analyses (*vide infra*), the synthesized Ag NPs after 60 min refluxing were largely composed of

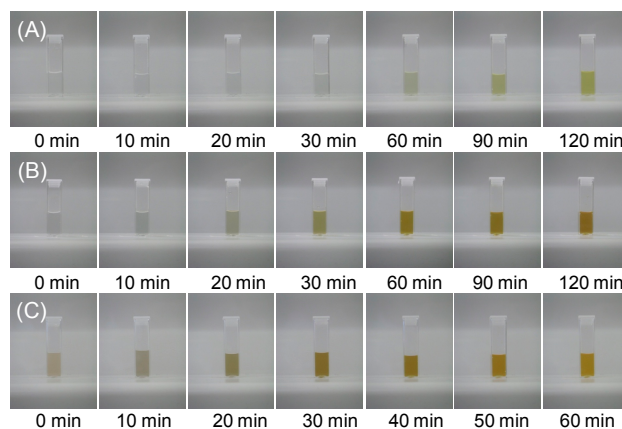


**Fig. 1** Time evolution of the color of the reaction solution in the cases of  $x =$  (A) 0, (B) 1.1, and (C) 3.6.

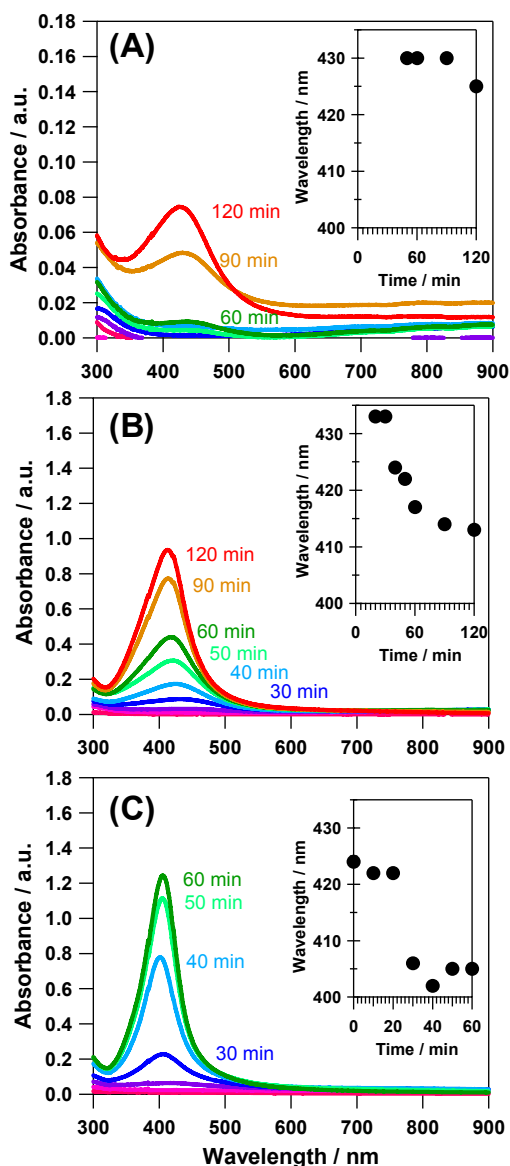


**Fig. 2** Time evolution of UV-vis spectra of the reaction solution in the cases of  $x =$  (A) 0, (B) 1.1, and (C) 3.6. The insets emphasize the shift of SPR peak wavelength as a function of refluxing time.

spherical Ag metal NPs with narrow size distribution (ca. 2–6 nm). Therefore, a blue shift in the SPR peak from 420–430 nm to 405–410 nm observed at an early stage of reaction in the cases of  $x = 1.1$  and 3.6 (Insets of Figs. 2B and 2C) indicates that the surface of small Ag seeds (such as clusters) is initially oxidized, and then, the conversion of surface oxide layer to Ag metal gradually occurred during refluxing. There is no red shift of the SPR peak wavelength during refluxing while the SPR peak intensity increases with extending the time of refluxing. Thus, the aggregation and further oxidation of synthesized Ag NPs could be ruled out during refluxing in water while the amount of Ag NPs increased in the solution.

In the case of  $x = 0$ , the same tendency is also observed, however the SPR peak intensity is quite small as shown in Fig. 2A. It is evident that the reaction rate is clearly different from

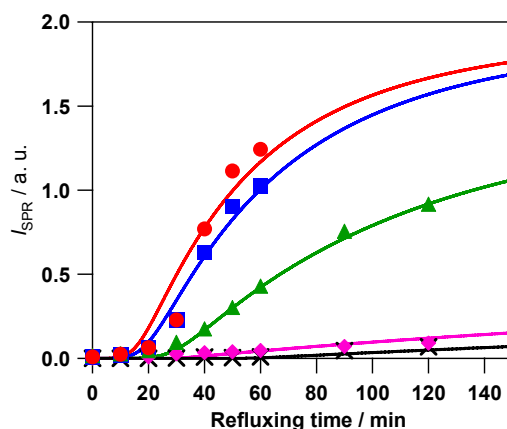


**Fig. 3** Time evolution of SPR intensity in the cases of  $x = 0$  ( $\times$ -mark), 0.4 (diamond), 1.1 (triangle), 1.8 (square), and 3.6 (circle). Solid lines represent the calculation results (*vide infra*).

the case of  $x \neq 0$ . The SPR peak intensity after 60 min refluxing in the case of  $x = 3.6$  is much higher than those of  $x = 1.1$  and 0. The positive correlation between  $x$  and the SPR peak intensity is clearly observed in all conditions (ESI, Fig. S2). It seems that NaOH has a large impact on the reaction kinetics of Ag NP formation, and causes an acceleration of the Ag NP formation when using dual active SA in water.

To evaluate the reaction kinetics during the Ag NPs formation using various amounts of NaOH, the changes in the intensity of the SPR band at 405 nm ( $I_{\text{SPR}}$ ) was plotted as a function of refluxing time (Fig. 3). In the case of  $x = 3.6$ ,  $I_{\text{SPR}}$  gradually increases from 0–20 min refluxing, and exponentially rose after 20 min refluxing. Therefore, there is an induction period in the initial stage of the reaction within 20 min time. In the cases of  $x = 1.8$  and 1.1, a similar behavior is observed, i.e., an induction period within 20 min followed by exponential increase (after 20 min) slightly descended with decreasing  $x$ . When  $x < 1.1$ , no exponential increase is observed, and thus, the induction period is indefinable. Even in the case of  $x = 0$ , however, a weak SPR band was seen after 60 min refluxing as shown in Fig. 2A, indicating that even in the absence of NaOH Ag NPs were formed, although only in small amount. In a separate study, a similar result was reported with respect to the Ag NPs formation,<sup>9</sup> and it was proposed that small seeds of  $\text{Ag}^0$  were formed during the first reaction step. These results indicate that Ag NPs gradually formed by refluxing the solution despite the amount of NaOH added, though the formation rate of Ag NPs strongly depends on the NaOH concentration. This suggests that NaOH accelerates the reduction reaction of  $\text{Ag}^+$  ions and/or the nucleation of Ag NPs.

### Structural characterization of products

Figure 4 shows the TEM images of the samples after refluxing for 60 min in the cases of  $x = 0, 1.1$  and 3.6. Many small NPs (ca. 2–6 nm) and a few large NPs (ca. 12 nm) can be seen in all images. The particle size distributions of all samples are almost the same and the mean diameter is ca. 3.5 nm. In the

case of  $x = 3.6$ , however, a small amount of large particles (ca. 12 nm) are formed as shown in Fig. 4C. Wang *et al.* studied the synthesis of PVP-capped Ag NPs using glucose and NaOH, and they observed that the NaOH had an adverse effect on particle agglomeration.<sup>16</sup> The large NPs observed in Fig. 4C might be produced by enhanced crystal growth and/or agglomeration of primary NPs. Though some large NPs were observed in all cases, no red shift in the SPR peak wavelength was detected during formation process (see the inset of Fig. 2). These results indicated that the number density of large NPs is negligible.

One question is why do the size distributions after 60 min refluxing show a similar tendency regardless of  $x$ , which has a major impact on the formation rate as discussed before. To provide an answer to the question, the coordination numbers (CN) of the samples after 60 min refluxing were estimated with the EXAFS analyses (shown in a later section). The CN is related to the mean diameter of NPs.<sup>17</sup> For example, CN = 10 corresponds to a metal NP of approximately 35 Å diameter based on the cuboctahedron model. The CNs of samples synthesized with  $x = 0, 1.1$  and  $3.6$  were CN = 0.7, 6.3 and 9.9, respectively. This result indicates the mean diameters of Ag NPs were below 35 Å in all cases. The diameter estimated from EXAFS analyses are averaged over all Ag atoms in the

solution. Thereby, these results imply that there are many ultra-small Ag clusters and/or Ag complexes, which conduce to small CNs, in all cases when comparing the mean sizes of Ag NPs estimated from TEM images.

The intensity of the SPR band for  $x = 3.6$  after 60 min refluxing was 146 times higher than that of  $x = 0$  (Fig. S2). Considering these results, the existence of small Ag<sup>0</sup> seeds (clusters and/or complexes), which could not be easily observed with TEM, were created in all conditions. Furthermore, in the case of  $x = 0$ , the fraction of Ag<sup>0</sup> seeds seems to be much higher than those of  $x = 1.1$  and  $3.6$ .

#### Kinetic rate consideration of Ag NP formation process

To consider the effect of NaOH, the rate of Ag NPs formation is analyzed based on a reaction kinetics study. For simplicity, in the reaction we assumed only reduction of Ag<sup>+</sup> ions and nucleation of Ag<sup>0</sup> neglecting the crystal growth. In our particular syntheses, the mean size of Ag NPs is unaffected by NaOH concentration (see Fig. 4), suggesting that the formation of NPs is dominated only by the nucleation process. Hence, the formation process of Ag NPs can be written by the following two-step reactions,



where  $k_1$  and  $k_2$  are overall reduction and nucleation rates, respectively. The rate equations can be expressed as

$$\frac{d[\text{Ag}^0]}{dt} = k_1[\text{Ag}^+] - nk_2[\text{Ag}^0]^n \quad (3)$$

$$\frac{d[\text{Ag}_n]}{dt} = k_2[\text{Ag}^0]^n \quad (4)$$

According to the results of XAFS analyses and TEM observations, there seems to be two main states of Ag intermediates, i.e., Ag<sup>+</sup> complexes (molecular state) and/or Ag<sup>0</sup> seeds (solid state) (*vide infra*). In general, the SPR intensity of metallic NPs is proportional to the cube of the NP diameter. Therefore, the contributions of Ag<sup>+</sup> complexes and ultra-small Ag clusters to the SPR intensity is negligible. The SPR intensity can be assumed to be proportional to the number of Ag NPs ( $I_{\text{SPR}} \propto [\text{Ag}_n]$ ), because the crystal growth has been neglected. In Fig. 3, the best fit curves obtained using Eqs. (3) and (4) are plotted as solid lines. As a result of the fitting, we observed that  $k_1$  and  $k_2$  increase with increasing the NaOH concentration, while  $n$  decreases with increasing the NaOH concentration (Fig. S3). This result clearly indicates that both the reduction reaction of Ag<sup>+</sup> and the nucleation of Ag NPs are simultaneously accelerated by NaOH. The chemical picture of the enhancement effect of the reaction rates will be discussed later.

#### Evaluation of XAFS spectra during Ag NP formation

To evaluate the state of Ag species at different points in the

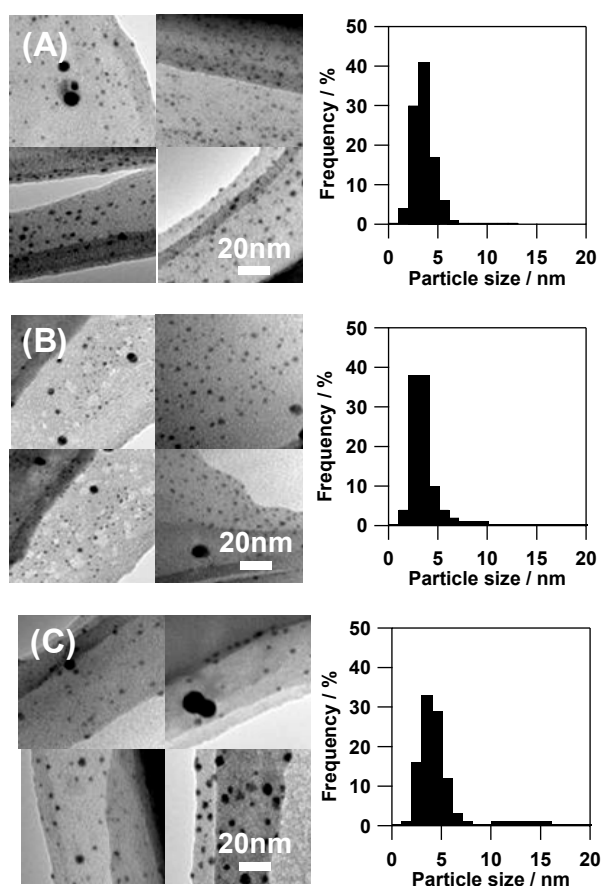


Fig. 4 TEM images of the samples after refluxing for 60 min in the cases of  $x =$  (A) 0, (B) 1.1, and (C) 3.6. The lower graphs correspond to the size distributions of NPs calculated from 800 randomly selected NPs from the TEM images.

reaction, the solutions collected by sampling were analyzed with the XAFS technique. Fig. 5 shows the X-ray absorption near-edge structure (XANES) spectra as a function of refluxing time,  $t$ , in the cases of  $x = 0, 1.1$  and  $3.6$ . The XANES spectra of reference materials such as Ag foil,  $\text{Ag}_2\text{O}$  powder, and  $\text{AgNO}_3$  (aq.) are shown in Fig. S4. The XANES spectrum at  $t = 0$  in the case of  $x = 0$  is almost identical to that of  $\text{AgNO}_3$  [Fig. 5A(i)]. On the other hand, the XANES spectrum at  $t = 0$  in the case of  $x = 3.6$  exhibits a two-humped peak that is characteristic of  $\text{Ag}_2\text{O}$  [Fig. 5C(i)]. According to the previous research,  $\text{Ag}^+$  ions were unstable in alkaline conditions ( $\text{pH} > 10.5$ ) and were converted to insoluble  $\text{Ag}_2\text{O}$  particles.<sup>18</sup> In our reaction conditions, the pH of the solution before refluxing is over 10.4 when  $x \geq 1.1$  (Fig. S5). Furthermore, the yellow color, XRD patterns and XAFS spectra of the samples before heating indicate the presence of  $\text{Ag}_2\text{O}$  phase (Figs. S6 and S7). Therefore, we can conclude that  $\text{Ag}_2\text{O}$  species were formed in the presence of NaOH, which serves as an alternative precursor accelerating the reduction reaction of  $\text{Ag}^+$  to  $\text{Ag}^0$ .

Taking a look at the time variations of XANES spectra, there were few qualitative differences in the case of  $x = 0$  (Fig. 5A). In the cases of  $x \neq 0$ , the XANES spectra gradually changed from a dampened structure to an undulated structure with increasing reflux time (Figs. 5B and 5C). This behavior indicates that the reduction from  $\text{AgNO}_3$  or  $\text{Ag}_2\text{O}$  to Ag metal is promoted by addition of NaOH, and the reduction rate depends on  $x$ .

To deeply elucidate the formation mechanism of Ag NPs, the time courses of  $|\text{FT}|$  of  $k^3\chi(k)$  is plotted in Fig. 6. It is known that  $\text{Ag}_2\text{O}$  has a peak at  $1.6 \text{ \AA}$  (Ag-O), while Ag metal

exhibits a peak at  $2.7 \text{ \AA}$  (Ag-Ag) (Fig. S4B). At  $t = 0$ , only the case of  $x = 3.6$  shows a significant  $|\text{FT}|$  peak at  $1.6 \text{ \AA}$  corresponding to the  $\text{Ag}_2\text{O}$  particles [Fig. 6C(i)], in which both cases of  $x = 0$  and  $1.1$  do not show a Ag-O peak at  $t = 0$  [Figs. 6A(i) and 6B(i)]. Note that both cases of  $x = 1.1$  and  $3.6$  before starting reflux indicated the Ag-O peaks as shown in Fig. S7. Hence, the formed  $\text{Ag}_2\text{O}$  NPs before heating might change into small Ag NPs or redissolve during the ramping of temperature in the case of  $x = 1.1$ . As shown in Fig. 6A, the case of  $x = 0$  exhibits no significant peak during refluxing. On the other hand, the cases of  $x = 1.1$  and  $3.6$  exhibit some characteristic peaks as shown in Figs. 6B and 6C. In the case of  $x = 1.1$ , the Ag-Ag peak gradually increased after 40 min refluxing [Fig. 6B(v)-(ix)]. In the case of  $x = 3.6$ , the Ag-Ag peak intensity increased with decrease in the Ag-O peak intensity as shown in Fig. 6C. This suggests that excess  $\text{Ag}_2\text{O}$  particles remained in the solution at  $t = 0$  due to the presence of much NaOH, and they were gradually transformed to Ag metal NPs during refluxing. According to these results, one of the roles of NaOH in the reaction is the production of insoluble  $\text{Ag}_2\text{O}$ , which creates another reaction pathway for formation of the Ag NPs with a much faster rate.

The transformation of the  $|\text{FT}|$  peak height at  $2.7 \text{ \AA}$ , which corresponds to the total number of Ag-Ag bonds in the system, were plotted as a function of refluxing time (Fig. 7). The peak height increases for extended refluxing, and the rate of increase positively correlates to  $x$ . These tendencies correspond to the results from UV-vis spectra (Fig. 3). These results strongly suggest that the reaction pathway is not only straightforward (i.e. directly *via*  $\text{AgNO}_3$  to Ag NP) but also

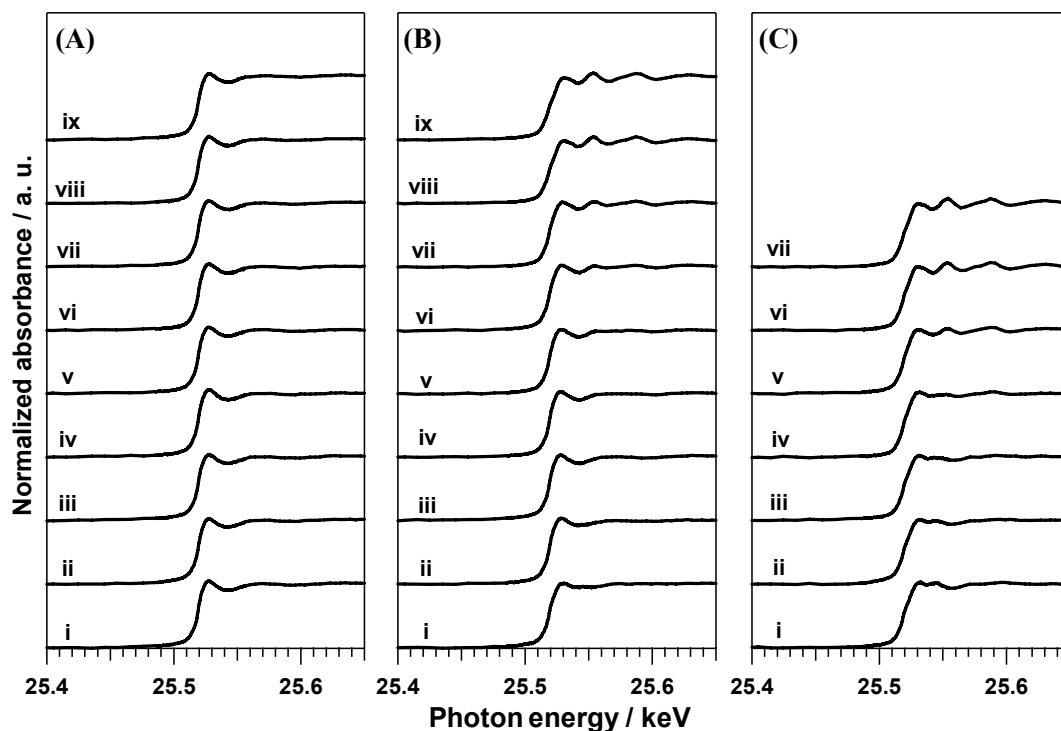


**Fig. 5** Time course of XANES spectra taken at (i) 0, (ii) 10, (iii) 20, (iv) 30, (v) 40, (vi) 50, (vii) 60, (viii) 90, and (ix) 120 min after starting reflux in the cases of  $x =$  (A) 0, (B) 1.1, and (C) 3.6.

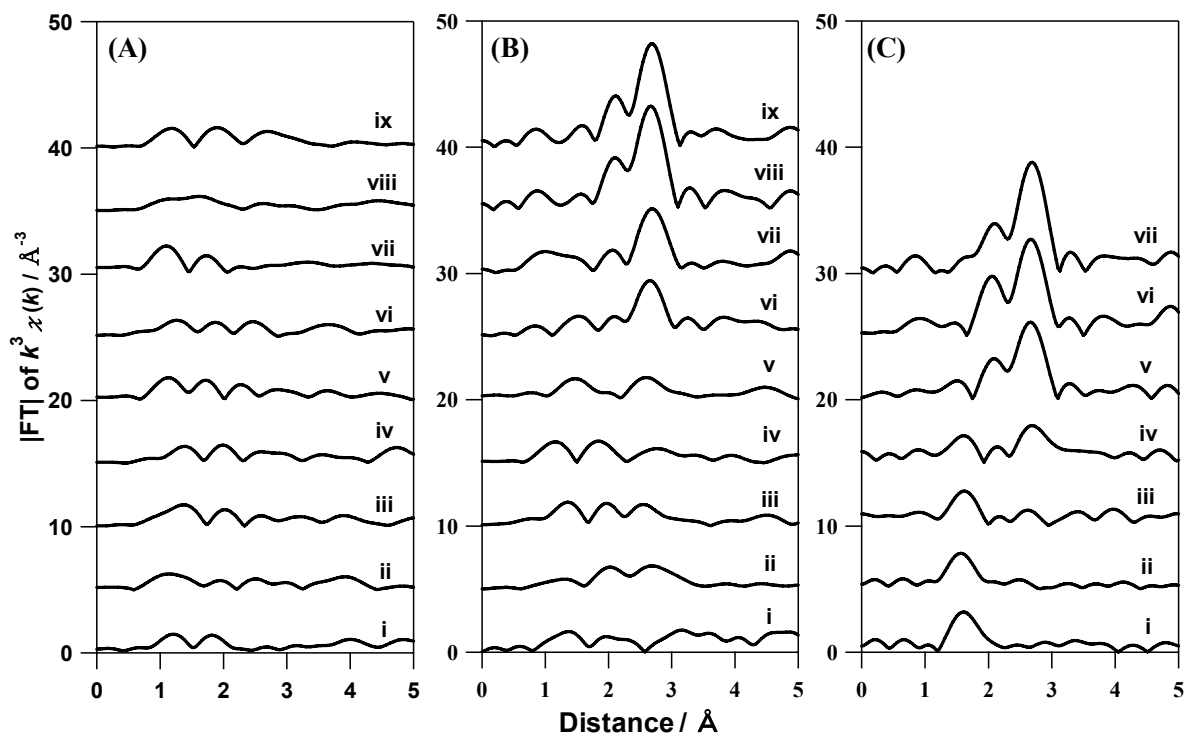


**Fig. 6** Time course of |FT| taken at (i) 0, (ii) 10, (iii) 20, (iv) 30, (v) 40, (vi) 50, (vii) 60, (viii) 90, and (ix) 120 min after starting reflux in the cases of  $x =$  (A) 0, (B) 1.1, and (C) 3.6.

occurs *via* the  $\text{Ag}_2\text{O}$  intermediate (at least in the case of  $x = 3.6$ ), which was created with NaOH. Evanoff *et al.* synthesized Ag NPs with hydrogen reduction of  $\text{Ag}_2\text{O}$ , and reported that  $\text{Ag}_2\text{O}$  as a precursor was more easily reduced than  $\text{AgNO}_3$ .<sup>19</sup> Guang-nian *et al.* proposed that the difference in reducing rate between  $\text{Ag}_2\text{O}$  and  $\text{AgNO}_3$  was due to the presence of  $\text{NO}_3^-$ .<sup>20</sup> However, neither of these studies mentions the complex intermediate formation observed in our own synthetic approach.

#### XANES study over the Ag NP formation

To clarify the intermediate state, the observed XANES spectra were deconvoluted using the reference spectra. Using Ockham's razor as an initial concept, we deconvoluted the observed XANES spectra with  $\text{AgNO}_3$  (aq.) and Ag foil spectra. If the least square error is always less than a threshold value for the cases of  $t = 0, 30$  and  $60$  min, we did not add another reference spectrum for the deconvolution. The least square error,  $R$ , is given as

$$R = \frac{\sum (X_{\text{obs}} - \sum \varphi_i X_i)^2}{\sum X_{\text{obs}}^2} \quad (5)$$

where  $X_{\text{obs}}$ ,  $X_i$  and  $\varphi_i$  are observed XANES spectrum, XANES spectrum of the  $i$ -th reference and contribution ratio of the  $i$ -th reference, respectively. Note that  $i = 1$  and  $2$  represent  $\text{AgNO}_3$  (aq.) and Ag foil spectra, respectively. The threshold value,  $R_{\text{th}}$ , is defined as  $0.025$ . If  $R > R_{\text{th}}$ , we added the  $\text{Ag}_2\text{O}$  spectrum as a third reference spectrum ( $i = 3$ ) for the deconvolution.

Figure 8 shows the results of the deconvolution of XANES spectra. In the cases of  $x = 0$  and  $0.4$ , the observed spectra could be well reproduced using two reference spectra ( $\text{AgNO}_3$  (aq.) and Ag foil) ( $R = 0.015$ – $0.022$ ). In the cases of  $x \geq 1.1$ ,  $\text{AgNO}_3$  (aq.) and Ag foil reference spectra were not enough to reproduce the observed spectra (i.e.  $R > R_{\text{th}}$ ) especially at an earlier stage of reaction as shown in Fig. 8C-E. Therefore, the

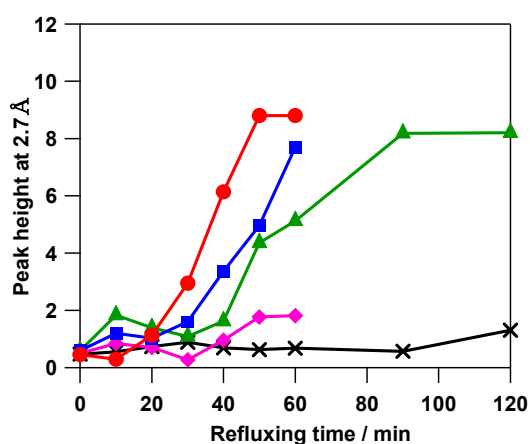


**Fig. 7** Time evolution of the height of |FT| at  $2.7 \text{ \AA}$  in the cases of  $x = 0$  ( $\times$ -mark),  $0.4$  (diamond),  $1.1$  (triangle),  $1.8$  (square), and  $3.6$  (circle).

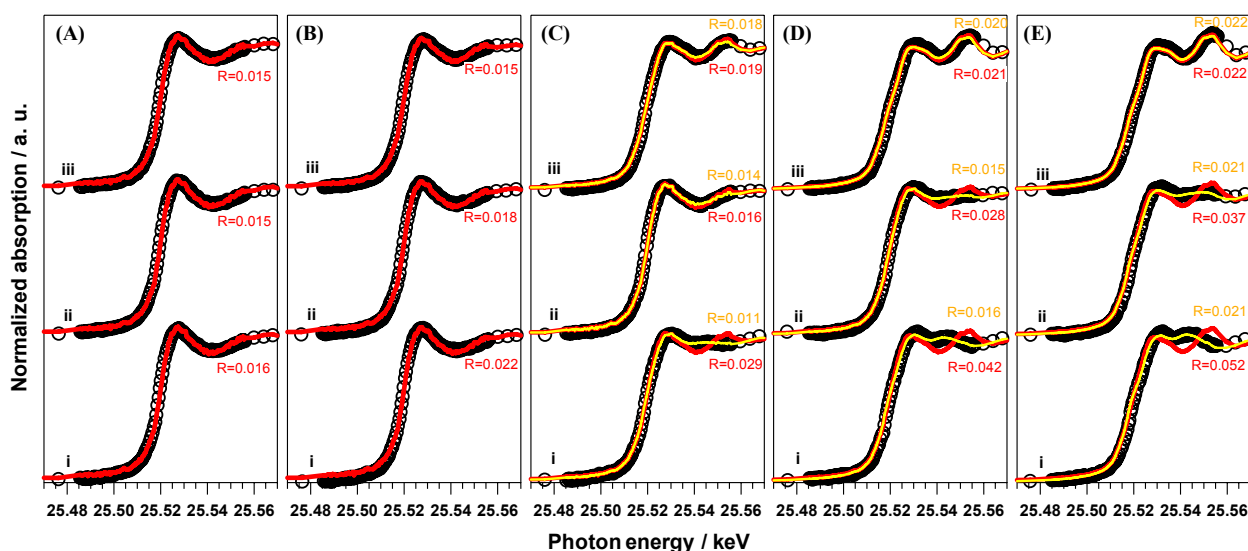


**Fig. 8** The observed and reconstructed XANES spectra at  $t =$  (i) 0, (ii) 30, and (iii) 60 min in the cases of  $x =$  (A) 0, (B) 0.4, (C) 1.1, (D) 1.8 and (E) 3.6. Black circles represent the observed XANES spectra. Red curves correspond to the sum spectra of  $\text{AgNO}_3$  (aq.) and Ag foil ( $\varphi_1 X_1 + \varphi_2 X_2$ ). Yellow curves correspond to the sum spectra of  $\text{AgNO}_3$  (aq.), Ag foil and  $\text{Ag}_2\text{O}$  ( $\varphi_1 X_1 + \varphi_2 X_2 + \varphi_3 X_3$ )

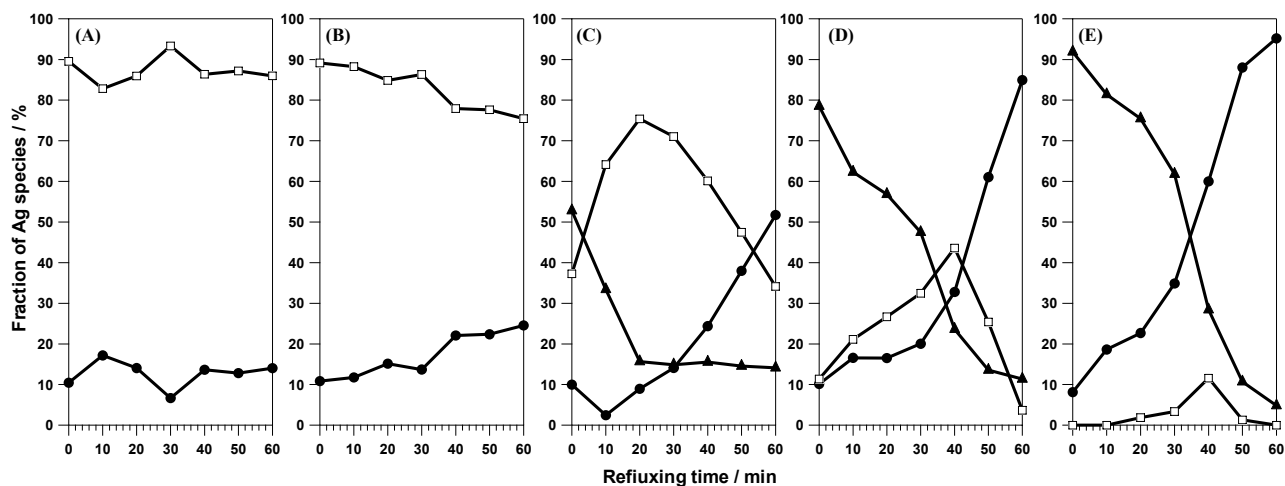


**Fig. 9** Time evolution of the fraction of each Ag species ( $\varphi$ ) in the cases of  $x =$  (A) 0, (B) 0.4, (C) 1.1, (D) 1.8, and (E) 3.6. Open squares, filled circles and filled triangles correspond to  $\varphi_1$  [ $\text{Ag}^+$  ( $\text{AgNO}_3$  origin)],  $\varphi_2$  (Ag metal) and  $\varphi_3$  [ $\text{Ag}^+$  ( $\text{Ag}_2\text{O}$  origin)], respectively.

$\text{Ag}_2\text{O}$  reference spectrum was taken into account. This assumption is reasonable because the XRD and EXAFS results clearly showed the existence of  $\text{Ag}_2\text{O}$  due to addition of a large amount of NaOH as noted before. As a result, the observed spectra could be well reproduced using three reference spectra ( $\text{AgNO}_3$  (aq.), Ag foil and  $\text{Ag}_2\text{O}$ ) in the cases of  $x \geq 1.1$  ( $R = 0.011$ – $0.022$ ).

Figure 9 shows the time evolution of  $\varphi_i$  during refluxing. In the case of  $x = 0$ , the transformation from  $\text{Ag}^+$  to Ag metal rarely happened as seen in Fig. 9A, indicating that the reduction reaction from  $\text{AgNO}_3$  to  $\text{Ag}^0$  NPs is a very slow process. In the case of  $x = 0.4$ , the reduction gradually proceeds to form trace amounts of Ag metal (Fig. 9B). In contrast, in the cases  $x = 1.1$  and 1.8, the fraction of  $\text{Ag}_2\text{O}$  species ( $\varphi_3$ ) is the highest at  $t = 0$ , and the fraction of  $\text{Ag}^+$  ( $\text{AgNO}_3$ ) ( $\varphi_1$ ) increase with decrease in  $\varphi_3$  at  $0 < t < 20$  min

for  $x = 1.1$  and at  $0 < t < 40$  min for  $x = 1.8$ . This implies the transformation of solid  $\text{Ag}_2\text{O}$  to  $\text{Ag}^+$ , which has similar electronic structure to  $\text{AgNO}_3$ , takes place at the initial stage of refluxing (Figs. 9C and 9D). After the initial increase,  $\varphi_1$  starts to decrease. At the same time,  $\varphi_2$  (Ag metal) starts to drastically increase. The transformation from  $\text{Ag}_2\text{O}$  to  $\text{Ag}^+$  and the reduction from  $\text{Ag}_2\text{O}$  to Ag metal seem to be competitive. In the case of  $x = 3.6$ ,  $\varphi_3$  is more than 90% at  $t = 0$  and  $\varphi_1$  maintains a low value throughout the reaction (Fig. 9E). This result seems to suggest that the reduction from  $\text{Ag}_2\text{O}$  to Ag metal are dominant compared to the transformation from  $\text{Ag}_2\text{O}$  to  $\text{Ag}^+$ . Importantly, the reduction rate notably increases with increase in  $x$ . The question arises here, why does the reduction rate of  $\text{Ag}^+$  to  $\text{Ag}^0$  increase with increasing  $x$  if  $\text{Ag}^+$  species created by redissolution of  $\text{Ag}_2\text{O}$  are the same as  $\text{AgNO}_3$ ? According to the aforementioned

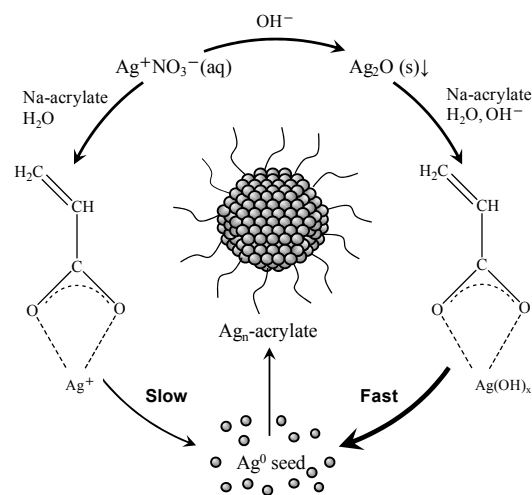
results, we speculate that an alternative  $\text{Ag}^+$  intermediate, which is of a different type from  $\text{AgNO}_3$  species, would be created in the reaction system when the NaOH concentration is high enough, because the rate of reduction reaction *via*  $\text{AgNO}_3$  to Ag NPs seems to be much slower than that of *via*  $\text{Ag}_2\text{O}$  as discussed in detail later.

### Proposed mechanism for the Ag NP formation

Here we summarize the following three important experimental facts: (1) insoluble  $\text{Ag}_2\text{O}$  particles are formed in the presence of NaOH at room temperature and the concentration of  $\text{Ag}_2\text{O}$  increases with increasing the NaOH concentration ( $x$ ), (2)  $\text{Ag}_2\text{O}$  particles redissolve during the heating (ramping of temperature and refluxing) creating  $\text{Ag}^+$  species, which has similar electronic structure to  $\text{AgNO}_3$ , and (3) both the reduction reaction of  $\text{Ag}^+$  and the nucleation of Ag NPs are simultaneously accelerated by increasing  $x$ .

In general, the state of complex and its reduction potential are varied depending on pH value.<sup>21</sup> For example, Au(III) or Pt(IV) complexes have different ligand-mediated structures depending on pH, and the reaction rates of the complexes to form NPs strongly depend on the molecular structures.<sup>22</sup> Wang *et al.* reported that a  $\text{Ag}(\text{OH})$  intermediate existed in the solution in the presence of NaOH.<sup>23</sup> The formation of  $\text{Ag}(\text{OH})_x$  through hydrolysis of  $\text{Ag}_2\text{O}$  was also proposed in the previous reports.<sup>19,24</sup> Considering the previous studies,  $\text{Ag}^+$  species created by redissolution of  $\text{Ag}_2\text{O}$  in our own experiments is in the form of  $\text{Ag}(\text{OH})_x$  such as  $\text{Ag}(\text{OH})$  and  $\text{Ag}(\text{OH})_2^-$ . Scheme 1 illustrates the proposed reaction pathways for the Ag NPs formation using SA as dual reducing and capping agents. According to a wide range of experimental results, we conclude that the following two reaction pathways exist in the system depending on  $x$ : (1) direct reduction of  $\text{Ag}^+$  ( $\text{AgNO}_3$  origin) to  $\text{Ag}^0$  followed by nucleation to form Ag NPs and (2) reduction of  $\text{Ag}(\text{OH})_x$ , which is formed from  $\text{Ag}_2\text{O}$  under alkaline conditions, to  $\text{Ag}^0$  followed by nucleation to form Ag NPs.

By the way, primary and secondary alcohol and aldehyde groups have been extensively used as a reducing agent in conjunction with base.<sup>25</sup> These functional groups are widely known as sacrificial oxidation agents by inducing the abstraction of  $\text{H}^+$  under alkaline condition.<sup>26</sup> Based on this fact, the reducing ability of SA is likely to be affected by NaOH. Carboxylic acid and salt, and amine groups also have been applied as a reducing agent.<sup>27</sup> Hoppe *et al.* suggested that the PVP degradation to the  $\text{H}^+$  and oxidation products after heating was observed.<sup>28</sup> The same phenomena were also suggested using ethylene glycol,<sup>29</sup> block-copolymer,<sup>30</sup> ascorbic acid,<sup>31</sup> vinyl group,<sup>32</sup> and *N,N*-dimethylformamide (DMF)<sup>33</sup> in the presence of alkaline additive. Therefore, these compounds act as a reducing agent in compensation for the oxidation of themselves. According to these results, NaOH might increase the reducing speed by accelerating the oxidation of the polymer by reducing the formed  $\text{H}^+$ . The observation of the decrease in the pH of the reaction solution after 60 min refluxing (Fig. S5) is presumably due to the formation of  $\text{H}^+$  with oxidation of SA. It is known that an increase in  $\text{H}^+$  concentration causes depression of reducing



Scheme 1. Reaction Scheme for the Ag NP Formation

activity of organic compounds in the case of the reducing reaction eliminating  $\text{H}^+$ .<sup>31</sup> This is because the standard redox potential is varied by pH. Therefore, it is highly possible that the reducing ability of SA is enhanced with increasing  $x$ .

In summary, there seems to be three possible reasons why both the reduction reaction of  $\text{Ag}^+$  and the nucleation of Ag NPs are simultaneously accelerated under alkaline condition. The first possible reason is that the reduction reaction takes place at the solid-liquid interface. The surfaces of solid  $\text{Ag}_2\text{O}$  particles are converted to  $\text{Ag}(\text{OH})_x$  during the ramping of temperature, and then, the reduction of  $\text{Ag}(\text{OH})_x$  by SA occurs on the  $\text{Ag}(\text{OH})_x$  surface followed by nucleation to form Ag NPs. The second possible reason is that the reduction rate constant itself of  $\text{Ag}(\text{OH})_x$  is much higher than that of  $\text{AgNO}_3$  even under the same conditions. The third possible reason is that the reducing ability of SA is enhanced with increasing pH. These might affect the reaction kinetics synergistically and the formation rate of Ag NPs dramatically increases with increasing the NaOH concentration.

## Conclusions

The role of NaOH on the reaction kinetics of Ag NPs formation were investigated using a wide variety of experimental/analytical techniques including UV-vis spectroscopy, TEM observation, XRD measurements, XAFS spectroscopy, and kinetic analyses. All results clearly indicate the existence of  $\text{Ag}_2\text{O}$  and  $\text{Ag}(\text{OH})_x$  as alternative intermediates when the NaOH concentration is high, which do not exist in the absence of NaOH. The possible reasons why the NaOH markedly accelerates the formation process of Ag NPs are found to be as follows: (1) the solid-liquid interface reaction, (2) the higher reduction rate constant of  $\text{Ag}(\text{OH})_x$ , and (3) the enhanced reducing ability of SA. Due to the dramatic increase in the reduction rate of  $\text{Ag}^+$ , the extremely-high supersaturation could be achieved on/near the surface of  $\text{Ag}_2\text{O}$  particles. As a result, the nucleation rate of Ag NPs is also significantly increased. The Ag nuclei diffuse into the

bulk solution. Presumably, due to a huge difference in the reduction rates between AgNO<sub>3</sub> in bulk solution and Ag(OH)<sub>x</sub> on/near the surface of solid Ag<sub>2</sub>O, the nucleation and growth processes might be separated autonomously. The clear separation between nucleation and growth processes might be a reason why the monodispersity of Ag NPs synthesized our own scheme becomes exceptionally high.

## Acknowledgements

We thank Mr. Kazuo Kato (JASRI) for assistance in using SSD instrument for XAFS measurement. The synchrotron radiation experiments have been performed at the BL01B1 station in the SPring-8 synchrotron radiation facility with the approval for young researcher's exploratory research (proposal No. 2010A1598) of the Japan Synchrotron Radiation Research Institute (JASRI).

## Notes and references

<sup>a</sup> School of Materials Science, Japan Advanced Institute of Science and Technology (JAIST), 1-1 Asahidai, Nomi, 923-1292, Japan. Fax: +81-761-51-1625; Tel: +81-761-51-1611; E-mail: shinya@jaist.ac.jp (S. M.), ebitani@jaist.ac.jp (K. E.)

<sup>b</sup> Department of Chemical System Engineering, School of Engineering, The University of Tokyo, 7-3-1 Hongo, Bunkyo-ku, Tokyo 113-8656, Japan.

† Electronic Supplementary Information (ESI) available: TEM, pH values, fitting results, XAFS, and XRD patterns. See DOI: 10.1039/b000000x/

- 1 G. Frens, *Nature*, 1973, **241**, 20; J. Turkevich, *Gold Bull.*, 1985, **18**, 86; S. Link, Z. L. Wang and M. A. El-Sayed, *J. Phys. Chem. B*, 1999, **103**, 3529; B. Lim, M. Jiang, J. Tao, P. H. C. Camargo, Y. Zhu and Y. Xia, *Adv. Funct. Mater.*, 2009, **19**, 189.
- 2 M. Yamada, Z. Shen and M. Miyake, *Chem. Commun.*, 2006, 2569; D. Lu, T. Qiu and X. L. Wu, *Eur. Phys. J. B*, 2004, **41**, 49.
- 3 M. Yamada, S. Kon and M. Miyake, *Chem. Lett.*, 2004, **34**, 1050; Z. Liu, Z. Hu, J. Liang, S. Li, Y. Ynag, S. Peng and Y. Quia, *Langmuir*, 2004, **20**, 214; B. Wiley, T. Herricks, Y. Sun and Y. Xia, *Nano Lett.*, 2004, **4**, 1733; J. Zeng, Y. Zheng, M. Rycenga, J. Tao, Z. Li, Q. Zhang, Y. Zhu and Y. Xia, *J. Am. Chem. Soc.*, 2010, **132**, 8552.
- 4 T. A. Ahmadi, Z. L. Wang, T. C. Green, A. Henglein and M. A. El-Sayed, *Science*, 1996, **272**, 1924; M. M. Koebel, L. C. Jones and G. A. Somorjai, *J. Nanopart. Res.*, 2008, **10**, 1063; J. Ohyama, Y. Hitomi, Y. Higuchi and T. Tanaka, *Top. Catal.*, 2009, **52**, 852.
- 5 J. Polte, T. T. Ahner, F. Delissen, S. Sokolov, F. Emmerling, A. F. Thunemann and R. Kraehnert, *J. Am. Chem. Soc.*, 2010, **132**, 1296.
- 6 M. Harada and Y. Inada, *Langmuir*, 2009, **25**, 6049; M. Harada, Y. Inada and M. Nomura, *J. Colloid Interface Sci.*, 2009, **337**, 427; M. Harada and H. Einaga, *Langmuir*, 2007, **23**, 6536; M. Harada and H. Einaga, *Langmuir*, 2006, **22**, 2371.
- 7 S. Nishimura, A. Takagaki, S. Maenosono and K. Ebitani, *Langmuir*, 2010, **26**, 4473; S. Nishimura, A. Takagaki, S. Maenosono and K. Ebitani, *NSTI-Nanotech.*, 2010, **1**, 356.
- 8 D. Mott, N. T. B. Thuy, Y. Aoki and S. Maenosono, *Phil. Trans. R. Soc. A*, 2010, **368**, 4275.
- 9 P. Silvert, R. Herrera-Urbina and K. Tekaiia-Elhssissen, *J. Mater. Chem.*, 1997, **7**, 293; I. Pastoriza-Santos and L. M. Liz-Marazan, *Langmuir*, 1999, **15**, 948; J. H. Kim, C. K. Kim, J. Won and Y. S. Kang, *J. Membr. Sci.*, 2005, **250**, 207.
- 10 D. L. V. Hyning and C. F. Zukoski, *Langmuir*, 1998, **14**, 7034.
- 11 Y. Yin, Z. Li, Z. Zhong, B. Gates, Y. Xia and S. Venkateswaeen, *J. Mater. Chem.*, 2002, **12**, 522.
- 12 K. G. Stamplecoskie and J. C. Scaiano, *J. Am. Chem. Soc.*, 2010, **132**, 1825; J. Zheng and R. M. Dickson, *J. Am. Chem. Soc.*, 2002, **124**, 13982; S. He, J. Yao, P. Jiang, D. Shi, H. Zhang, S. Xie, S. Pang and H. Gao, *Langmuir*, 2001, **17**, 1571.
- 13 J. M. Nedeljkovic and V. V. Vukovic, *Langmuir*, 1993, **9**, 980; S. Kapoor, *Langmuir*, 1998, **14**, 1021; T. Pal; T. K. Sau and N. R. Jana, *Langmuir*, 1997, **13**, 1481.
- 14 T. Pal; T. K. Sau and N. R. Jana, *Langmuir*, 1997, **13**, 1481.
- 15 J. J. Mock, M. Barbic D. R. Smith, D. A. Schultz and S. Schultz, *J. Chem. Phys.*, 2002, **116**, 6755; R. Zong, J. Zhou, Q. Li, B. Du, B. Li, M. Fu, X. Qi, L. Li and S. Buddhudu, *J. Phys. Chem. B*, 2004, **108**, 16713.
- 16 H. Wang, X. Qiao, J. Chen and S. Ding, *Colloids Surf. A: Physicochem. Eng. Aspects*, 2005, **256**, 111.
- 17 A. I. Frenkel, C. W. Hills and R. G. Nuzzo, *J. Phys. Chem. B*, 2001, **105**, 12689; A. Jentys, *Phys. Chem. Chem. Phys.*, 1999, **1**, 4059; J. Graaf, A. J. Dillen, K. P. Jong and D. C. Koningsberger, *J. Catal.*, 2001, **203**, 307.
- 18 B. J. Murray, Q. Li, J. T. Newberg, E. J. Menke, J. C. Hemminger and R. M. Penner, *Nano Lett.*, 2005, **5**, 2319.
- 19 D. D. Evanoff and G. Chumanov, *J. Phys. Chem. B*, 2004, **108**, 13948.
- 20 X. Guang-nian, Q. Xue-liang, Q. Xiao-lin and C. Jian-guo, *Colloids Surf. A: Physicochem. Eng. Aspects*, 2008, **320**, 222.
- 21 D. Krishnan and T. Pradeep, *J. Cryst. Growth*, 2009, **311**, 3889.
- 22 X. Ji, X. Song, J. Li, Y. Bai, W. Yang and X. Peng, *J. Am. Chem. Soc.*, 2007, **129**, 13939; F. Zhang, J. Chen, X. Zhang, W. Gao, R. Jin, N. Guan and Y. Li, *Langmuir*, 2004, **20**, 9329; B. J. Morrow, E. Matijevic and D. V. Goia, *J. Colloid Interface Sci.*, 2009, **335**, 62.
- 23 X. Wang, H. Wu, Q. Kuang, R. Huang, Z. Xie and L. Zheng, *Langmuir*, 2010, **26**, 2774.
- 24 G. Biedermann and L. G. Sillen, *Acta Chem. Scand.*, 1960, **14**, 717.
- 25 H. Wang, X. Qiao, J. Chen, X. Wang and S. Ding, *Mater. Chem. Phys.*, 2005, **94**, 449; K. Chou and C. Ren, *Mater. Chem. Phys.*, 2000, **64**, 241; S. L. Hsu and R. Wu, *Mater. Lett.*, 2007, **61**, 3719; B. He, J. J. Tan, K. Y. Liew and H. Liu, *J. Mol. Catal. A: Chem.*, 2004, **221**, 121.
- 26 T. Mitsudome, A. Noujima, T. Mizugaki, K. Jitsukawa and K. Kaneda, *Green Chem.*, 2009, **11**, 793; K. Ebitani, K. Motokura, T. Mizugaki and K. Kaneda, *Angew. Chem., Int. Ed.*, 2005, **44**, 3423; K. Ebitani, K. Motokura, K. Mori, T. Mizugaki and K. Kaneda, *J. Org. Chem.*, 2006, **71**, 5440.
- 27 I. Hussain, M. Brust, A. J. Papworth and A. I. Cooper, *Langmuir*, 2003, **19**, 4831; R. Sardar, J. Park and J. S. Shumaker-Parry, *Langmuir*, 2007, **23**, 11883; P. N. Njoki, I. S. Lim, D. Mott, H. Park, B. Khan, S. Mishra, R. Sujakumar, J. Luo and C. Zhong, *J. Phys. Chem. C*, 2007, **111**, 14664; I. Washio, Y. Xiong, Y. Yin and Y. Xia, *Adv. Mater.*, 2006, **18**, 1745.
- 28 C. E. Hoppe, M. Lazzari, I. Pardinas-Blanco and M. A. Lopez-Quintela, *Langmuir*, 2006, **22**, 7027.
- 29 L. Longenberger and G. Mills, *J. Phys. Chem.*, 1995, **99**, 475; Y. Sun, Y. Yin, B. T. Mayers, T. Herricks and Y. Xia, *Chem. Mater.*, 2002, **14**, 4736.
- 30 T. Sakai and P. Alexandrides, *J. Phys. Chem. B*, 2005, **109**, 7766.
- 31 I. Sondi, D. V. Goia and E. Matijevic, *J. Colloid Interface Sci.*, 2003, **260**, 75; D. V. Goia and E. Matijevic, *Colloids Surf. A: Physicochem. Eng. Aspects*, 1999, **146**, 139.
- 32 M. S. Yavuz, W. Li and Y. Xia, *Chem. Eur. J.*, 2009, **15**, 13181.
- 33 I. Pastoriza-Santos and L. M. Liz-Marzan, *Langmuir*, 1999, **15**, 948.